Electronic Supplementary Information

In vitro simultaneous mapping of the partial pressure of oxygen, pH and inorganic phosphate using electron paramagnetic resonance

Akihiro Taguchi,[a] Stephen DeVience,[b,c] Benoit Driesschaert,[b,d] Valery V. Khramtsov[b,c] and Hiroshi Hirata*[e]

[a] Division of Bioengineering and Bioinformatics, Graduate School of Information Science and Technology, Hokkaido University, North 14, West 9, Kita-ku, Sapporo, 060-0814, Japan

[b] In Vivo Multifunctional Magnetic Resonance centre, West Virginia University, Robert C. Byrd Health Sciences Centre, 1 Medical Centre Drive, Morgantown, West Virginia 26506, USA

[c] Department of Biochemistry, School of Medicine, West Virginia University, Morgantown, WV, 26506, USA

[d] Department of Pharmaceutical Sciences, School of Pharmacy, West Virginia University, Morgantown, WV, 26506, USA

[e] Division of Bioengineering and Bioinformatics, Faculty of Information Science and Technology, Hokkaido University, North 14, West 9, Kita-ku, Sapporo, 060-0814, Japan

* E-mail: hhirata@ist.hokudai.ac.jp

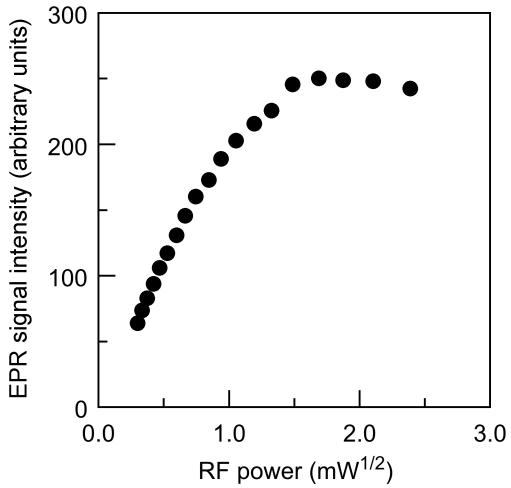

Fig. S1 RF power saturation characteristics of the signal intensity for p_1TAM-D. The measurement parameters of the spectrum were as follows: magnetic field scanning 0.8 mT, magnetic field modulation 8 μT, scan duration 100 ms, the time constant of lack-in amplifier 30 μs, the number of data points per scan 2048 and the number of averaging 300. The RF magnetic field generation coefficient of the RF resonator was 98 $\mu T/W^{1/2}$.

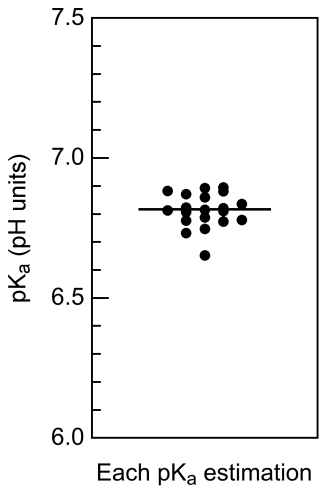

Fig. S2 The scatter of acid dissociation constant pK_a estimation. The mean of estimated pK_a values was obtained from 20 EPR spectra with different sample pH values. The bar in the plot (6.81) shows the mean of the pK_a plots. The standard deviation was estimated to be 0.061 pH units, and the standard error of the mean was estimated to be 0.014 pH units (sample size n = 20). Each plot (pK_a) was obtained from the measured fraction P_a and the known-sample pH value. In this measurement, dissolved oxygen was purged by nitrogen gas bubbling, and the measurements were performed at room temperature (25ºC).

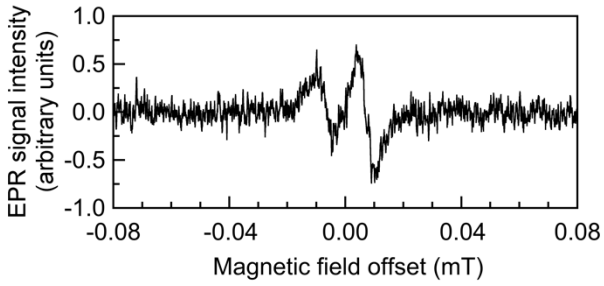

Fig. S3 Representative zero-gradient EPR spectrum for the multiple conditioned p_1TAM-D solutions. This spectrum was recorded from the samples shown in Fig. 3 with a single accumulation (scan duration of 0.1 s). The measurement parameters are given in Experimental section (EPR spectroscopy and imaging). The signal-to-noise ratio of this spectrum was estimated to be 7.5. The noise amplitude was given as the two-fold root-mean-square value of the baseline noise, which was obtained from the 200 data points at the left end of the spectrum.

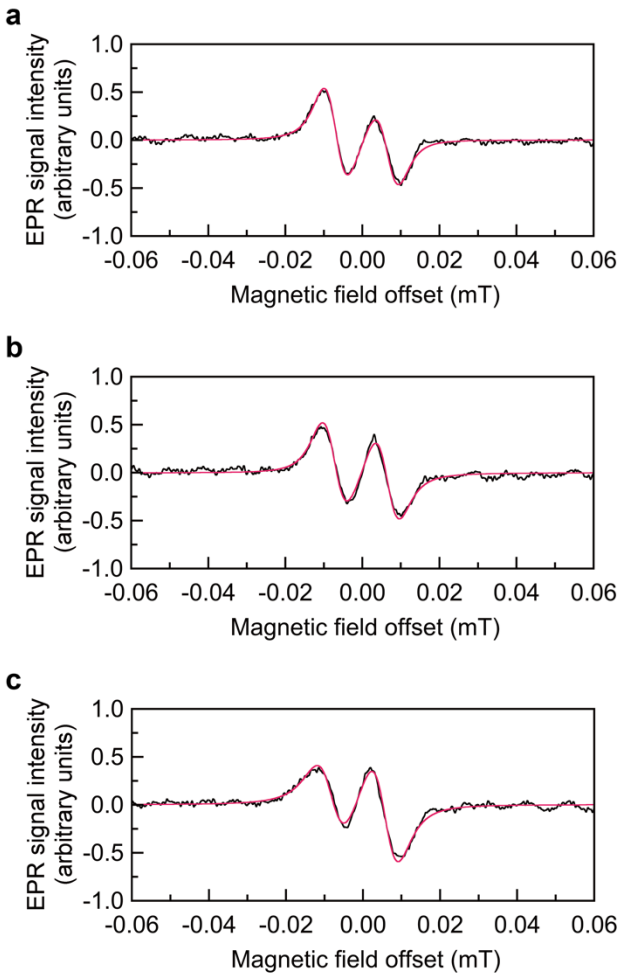

Fig. S4 Representative EPR spectra for the multiple conditioned p_1TAM-D solutions. EPR spectra at the specified voxels (almost the centre of each tube) in the tube #4 (a), #5 (b) and #6 (c). Black and red lines represent reconstructed EPR spectra and corresponding fitted spectra, respectively. The prepared conditions were pO_2 = 0 mmHg, pH=6.70 and Pi=4.0 mM in the tube #4; pO_2 = 19 mmHg, pH = 6.78 and Pi = 2.5 mM in the tube #5; pO_2 = 38 mmHg, pH = 6.90 and Pi = 1.25 mM in the tube #6. The concentration of NaCl was 38 mM for three samples. The spectral lineshape at each voxel derives the pO_2, pH and Pi values with the predetermined calibration curves.

Table S1 Comparison of imaging modalities for the partial pressure of oxygen, pH and inorganic phosphate in biomedical applications.

Imaging modalities	pO_2		pH		Pi	
	Pros	Cons	Pros	Cons	Pros	Cons
^{19}F-MRI	• Preclinical use • Clinical scanner available	• Low sensitivity • High concentration of the probe				
BOLD MRI	• Clinically applicable • Availability of ^{1}H MRI anatomical co-imaging	• Indirect assessment of oxygen (blood flow/deoxyhemoglobin content)				
MOBILE MRI	• Clinically applicable • Availability of ^{1}H MRI anatomical co-imaging	• Qualitative assessment of hypoxic areas				
^{18}F-MISO PET	• High detection sensitivity • Clinically available • Hypoxic cell targeting	• Radioactive tracer • Non-linear response to pO_2				
Fluorescent/ phosphorescent imaging	• High spatial resolution	• Limited penetration depth	• High spatial resolution	• Limited penetration depth		
Near-infrared spectroscopy and imaging	• Clinically applicable	• Not detecting pO_2 (detecting oxygen saturation)				
Photo-acoustic imaging	• Larger imaging depth than Fluorescent imaging	• Difficult to quantify pO_2				
(acido) CEST-MRI			• Clinically available • CT agents (e.g., iopamidol) applicable to IV delivery • Availability of ^{1}H MRI anatomical co-imaging	• Low sensitivity		
^{31}P-NMR/MRI			• Specific detection of extracellular pH using exogenous ^{31}P probes	• Low sensitivity	• No imaging agent required	• Low detection sensitivity • Difficulties to discriminate intra and extracellular Pi
Hyperpolarized ^{13}C-MRI			• Clinical scanner available	• Limited acquisition time/measure-ment time • Hyper-polarizer required		
OMRI (PEDRI)	• Good spatial resolution • Concurrency using multiple scans • Availability of ^{1}H MRI anatomical co-imaging	• High RF power absorption	• Good spatial resolution • Concurrency using multiple scans • Specific detection of extracellular pH	• High RF power absorption	• Good spatial resolution • Concurrency using multiple scans • Specific detection of extracellular Pi	• High RF power absorption
EPR*	• High accuracy and sensitivity to absolute values of oxygen concentration • Concurrency using multi-functional pTAM probe	• Concentration-induced line broadening • Moderate resolution *in vitro* • Intra-tissue delivery of pTAM probe *in vivo*	• Specific detection of extracellular pH • Good accuracy • Concurrency using pTAM probe	• Intra-tissue delivery of pTAM probe, *in vivo*	• Specific detection of extracellular Pi • Concurrency using pTAM probe	• Moderate resolution *in vitro* • Intra-tissue delivery of pTAM probe, *in vivo*

Note: IV stands for 'intravenous' route. * Faster acquisition required for 3D mapping (CW-EPR).

Table S2 The measured values of the partial pressure of oxygen, pH and inorganic phosphate for sample No. 4 (Fig. 5) with different threshold levels (mean ± SD).

Threshold level (%)	Number of voxels	pO_2 (mmHg)	pH	Pi (mM)
90	73	4 ± 5	6.70 ± 0.01	4.2 ± 0.2
80	174	4 ± 5	6.70 ± 0.01	4.2 ± 0.3
70	285	5 ± 5	6.70 ± 0.01	4.1 ± 0.3
60	427	5 ± 5	6.70 ± 0.01	4.1 ± 0.3
50	608	5 ± 5	6.70 ± 0.01	4.1 ± 0.4
40	834	5 ± 5	6.70 ± 0.01	4.1 ± 0.4
30	1244	5 ± 5	6.70 ± 0.01	4.0 ± 0.4
20	1749	5 ± 5	6.70 ± 0.01	4.0 ± 0.4

Table S3 The measured values of the partial pressure of oxygen, pH and inorganic phosphate for sample No. 5 (Fig. 5) with different threshold levels (mean ± SD).

Threshold level (%)	Number of voxels	pO_2 (mmHg)	pH	Pi (mM)
90	---	---	---	---
80	---	---	---	---
70	31	23 ± 3	6.75 ± 0.01	2.4 ± 0.4
60	142	22 ± 4	6.75 ± 0.01	2.3 ± 0.4
50	304	22 ± 5	6.75 ± 0.01	2.3 ± 0.4
40	520	21 ± 5	6.76 ± 0.01	2.3 ± 0.5
30	850	21 ± 5	6.76 ± 0.01	2.3 ± 0.5
20	1433	21 ± 6	6.76 ± 0.01	2.3 ± 0.6

Table S4 The measured values of the partial pressure of oxygen, pH and inorganic phosphate in sample No. 6 (Fig. 5) with different threshold levels (mean ± SD).

Threshold level (%)	Number of voxels	pO_2 (mmHg)	pH	Pi (mM)
90	---	---	---	---
80	29	56 ± 5	6.87 ± 0.01	1.3 ± 0.2
70	161	49 ± 9	6.88 ± 0.01	1.6 ± 0.4
60	346	47 ± 9	6.88 ± 0.01	1.5 ± 0.4
50	558	45 ± 10	6.88 ± 0.02	1.5 ± 0.5
40	830	43 ± 10	6.88 ± 0.02	1.5 ± 0.5
30	1170	42 ± 10	6.88 ± 0.02	1.5 ± 0.6
20	1616	41 ± 10	6.88 ± 0.02	1.5 ± 0.6

Note: These values in Tables S2 to S4 were obtained from the middle half of the reconstructed data (36 out of 72 slice images).